Cell Reports
Article

Cell PRESS
Open ACCESS

Septin-Containing Barriers Control the Differential Inheritance of Cytoplasmic Elements

Alan Michael Tartakoff,[1,*] Ilya Aylyarov,[1] and Purnima Jaiswal[1]
[1]Pathology Department and Cell Biology Program, Case Western Reserve University, 2103 Cornell Road, Cleveland, OH 44106, USA
*Correspondence: amt10@case.edu
http://dx.doi.org/10.1016/j.celrep.2012.11.022

SUMMARY

Fusion of haploid cells of *Saccharomyces cerevisiae* generates zygotes. We observe that the zygote midzone includes a septin annulus and differentially affects redistribution of supramolecular complexes and organelles. Redistribution across the midzone of supramolecular complexes (polysomes and Sup35p-GFP [PSI+]) is unexpectedly delayed relative to soluble proteins; however, in [*psi*-] × [*PSI*+] crosses, all buds eventually receive Sup35p-GFP [*PSI*+]. Encounter between parental mitochondria is further delayed until septins relocate to the bud site, where they are required for repolarization of the actin cytoskeleton. This delay allows rationalization of the longstanding observation that terminal zygotic buds preferentially inherit a single mitochondrial genotype. The rate of redistribution of complexes and organelles determines whether their inheritance will be uniform.

INTRODUCTION

Asymmetric cell division can occur if the two ends of the spindle reside in compositionally distinct regions of the cytoplasm (Barral and Liakopoulos, 2009; Knoblich, 2008; Pereira and Yamashita, 2011; Rando, 2006; Rujano et al., 2006). The present study is concerned with the causes of such inhomogeneity, using as a model the elongated zygotes of *Saccharomyces cerevisiae* that result from fusion of haploid cells. When buds form at the termini of zygotes, buds that emerge at the corresponding end preferentially inherit the mitochondrial genomes contributed by a single parent (Birky, 1975; Dujon, 1981; Lukins et al., 1973; Nunnari et al., 1997; Okamoto and Shaw, 2005; Strausberg and Perlman, 1978). A partial explanation of this asymmetry is provided by the observation that, although nuclei congress and fuse soon after cell-cell fusion (Melloy et al., 2007; Molk and Bloom, 2006; Tartakoff and Jaiswal, 2009), parental mitochondria encounter and fuse with each other in the midzone of the zygote significantly later (Hoppins et al., 2007; Nunnari et al., 1997; Okamoto et al., 1998). Mechanisms underlying this genetic and cell biological puzzle have not been investigated.

These considerations also provide a point of reference for understanding the distribution and mitotic inheritance of supramolecular complexes, including the prion form of Sup35p. When in the [*psi*$^-$] conformation, Sup35p acts as a translation termination factor. In an alternate ("aggregated") conformer prion form(s), [*PSI*$^+$] self-associates and allows read-through of termination codons. [*PSI*$^+$] can template the conversion of [*psi*$^-$] to [*PSI*$^+$], and monomeric-oligomeric forms of Sup35p interconvert in [*PSI*$^+$] cells (Cox et al., 1988; Liebman and Chernoff, 2012; Paushkin et al., 1996; Serio and Lindquist, 1999; Wickner et al., 2007). Several prions, both in fungi and in mammalian cells, are toxic (Halfmann et al., 2011; Mathur et al., 2012; McGlinchey et al., 2011; Vishveshwara et al., 2009; Wickner et al., 2010). Moreover, some can form macroscopic aggregates that reduce mitotic inheritance, as do certain oxidized proteins (Aguilaniu et al., 2003; Bagriantsev et al., 2008; Derdowski et al., 2010; Erjavec et al., 2007; Tyedmers et al., 2010; Uptain et al., 2001). By visualizing Sup35p tagged with green fluorescent protein (GFP) contributed by one parent during zygote formation, one can investigate the timing of its aggregation and its transmission. Barriers within the zygote could restrict these events.

In mitotic yeast, a cortical patch or ring of five septins (Cdc3, Cdc10, Cdc11, Cdc12, and Shs1) accumulates along with the myosin, Myo1p, at the site of the incipient bud. This unit then forms an hourglass-like structure that encircles the bud neck. Prior to cytokinesis, the hourglass is replaced by two rings; a further ring of actin forms between these rings, and contraction of this unit promotes cytokinesis (Bi et al., 1998; Caudron and Barral, 2009; Lippincott et al., 2001; Longtine and Bi, 2003; Spiliotis and Gladfelter, 2012). A "fence" function of septins in which they limit diffusion of cortical proteins has been described at the bud neck (Caudron and Barral, 2009; Longtine and Bi, 2003). The present study considerably extends the significance of septins by showing that a septin-containing partition subcompartmentalizes noncortical portions of the zygote cytoplasm. Moreover, relocation of septins to the site of bud formation promotes polarization of the actin cytoskeleton.

The nonuniform distribution of components of mammalian cells could be limited by barriers equivalent to those that we characterize in this study. Moreover, the yeast bud neck resembles the cytokinetic bridge of animal cells. Both structures include septins and actin (Balasubramanian et al., 2004; Estey et al., 2010; Hurley and Hanson, 2010; Liu et al., 2012; Seshan and Amon, 2004; Steigemann et al., 2009).

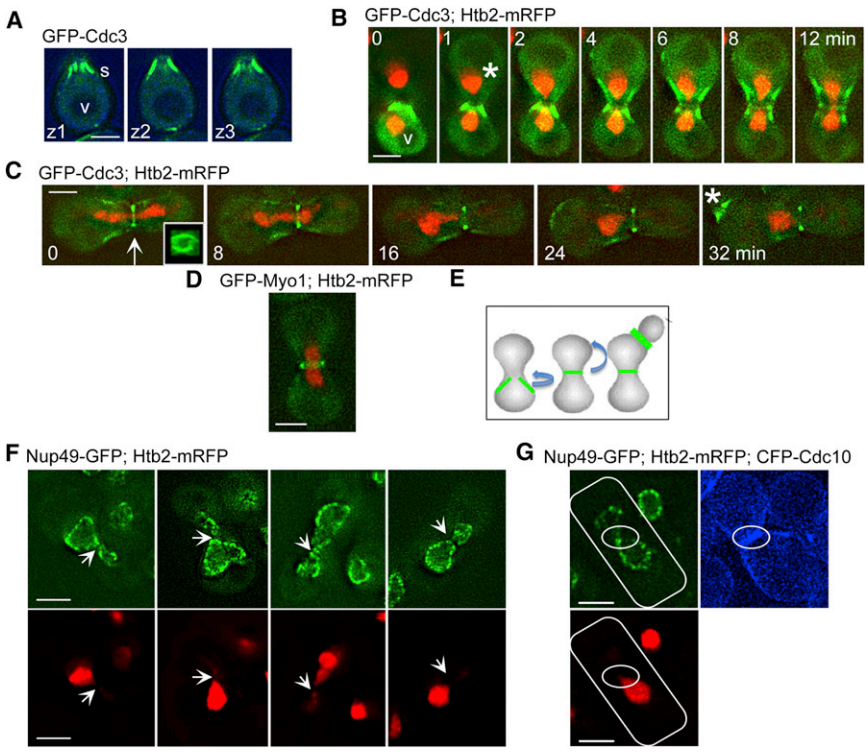

Figure 1. Septin Morphogenesis

(A) Septin distribution in mating projections. Cells expressing the tagged septin, GFP-Cdc3p, were treated with 30 μM α-factor for 3 hr. A through-focal series (z1–z3, 0.4 μ each) shows that the cortical signal extends toward but does not reach as far as the apex of the cell. S, septin; V, vacuole. Strain: ATY3432. Scale bar represents 5 microns in all figures.

(B) *cis-trans* redistribution of septins. A strain expressing the tagged histone, Htb2p-mRFP, as well as GFP-Cdc3p (lower cell) was crossed with a strain expressing Htb2p-mRFP (upper cell). Note the transfer of the diffuse cytoplasmic GFP-Cdc3p signal (1 min time point, *), and the progressive appearance of the labeled collar at the cell cortex in the *trans* parental domain (4–12 min time points). In the final images, the medial annulus begins to appear perpendicular to the long axis of the zygote. Strains: ATY3432 × ATY2289.

(C) Appearance of the annulus. As in Figure 1B, a strain expressing the tagged histone, Htb2p-mRFP, as well as GFP-Cdc3p was crossed with a strain expressing Htb2p-mRFP. Note the collar at early time points and the medial transverse GFP-positive annulus (arrow) through which the nuclei fuse. At later time points (24 and 32 min), the collar becomes weaker and a patch of Cdc3p-GFP appears at the site of formation of a terminal bud (*). The insert in the first panel shows a face view of the annulus from an early time point. Strains: ATY3432 × ATY2289.

(D) The myosin, Myo1p, is present in the midzone. Two strains expressing GFP-Myo1p (one of which expresses Htb2p-mRFP) were crossed. Note the transverse medial signal and the lack of cortical signal. Strains: ATY3431 × ATY3437.

(E) Model of septin morphogenesis. We propose that the initial cortical signal progressively is replaced by the medial annulus and finally by septin accumulation at the bud neck.

(F) Position of the nuclear envelope after consolidation of chromatin. Two strains expressing the tagged nucleoporin, Nup49p-GFP, and Htb2p-mRFP were crossed. Zygotes were examined when most of the chromatin had moved aside from the midpoint, which is designated by the arrows. A significant amount of the nuclear envelope lies in the opposite lobe from chromatin. Note that the exact midpoint (arrowheads) generally lacks nuclear pore complexes. The images that include histones have been separated from those that illustrate the nuclear pores. Strains: ATY2594 × ATY3358.

(G) Distribution of septins when the nuclear envelope spans the midpoint. A cross equivalent to that illustrated in (F) was conducted between a strain expressing Htb2p-mRFP and Nup49p-GFP (lower cell) and a strain expressing the tagged septin, Cdc10p-CFP (upper cell). The three images are of the same zygote. Note that when chromatin is on one side of the midpoint, the narrowed midpoint (circled) coincides with the blue septin annulus. Strains: ATY3358 × ATY4003.

See also Figure S1.

A further point of interest in studying zygotes pertains to transgenerational inheritance. In cells that result from fusion of distinct precursors, if mitosis occurs before thorough mixing of parental complexes and organelles, distinct characteristics can be passed to subsets of progeny (i.e., from an initial generation to the third generation).

RESULTS

Five Steps of Septin Morphogenesis during Zygote Formation

When haploid yeast of opposite mating type are mixed at room temperature, zygotes form after 1.5–2.0 hr. To establish the relative timing of *cis*-to-*trans* redistribution of parental proteins and organelles, we used time-lapse microscopy and visualized fluorescent marker proteins. Population-based estimates of relative timing agree with time-lapse observations, but the temporal dispersion of these events makes it more informative to use time-lapse, which also can illustrate the suddenness of redistribution. The selected images and time-lapse series illustrated below are in all cases representative of examination of at least twenty cells.

We initially observed that redistribution of distinct organelles and supramolecular complexes is by no means synchronous. We therefore have inquired whether cytoskeletal barriers partition the cytoplasm, beginning with septins.

After treatment of MAT a haploid cells with mating factor for 2–3 hr, the tagged septin, GFP-Cdc3p, forms a collar at the cell cortex distal to the tip of the mating projection, as previously described (Ford and Pringle, 1991; Kim et al., 1991; Longtine et al., 1998) (Figure 1A). This collar has a composite organization in which lobes are joined at their apical ends and become increasingly splayed as they extend distally. A pool of diffuse cytoplasmic fluorescence is also evident.

When a mating pair meets, the two plasma membranes form a flattened "zone of contact" (Byers and Goetsch, 1975). In crosses in which one partner expresses GFP-Cdc3p, contact is followed by entry of a diffuse signal into the acceptor cell.

Within 5 min, the collar in the acceptor cell then becomes symmetrically labeled (Figure 1B, 4–6 min time points). Such behavior is expected if a soluble pool of GFP-Cdc3p permeates *cis* to *trans*, and if assembly of the collar is dynamic.

Just prior to nuclear contact, a GFP-Cdc3p-positive structure appears at the interface between the two parental domains (e.g., Figures 1B and 1C). It can also be detected in cells expressing other tagged septins (GFP-Cdc10p, GFP-Cdc11p, or GFP-Cdc12p) (not shown). In face view, it appears as an annulus (Figure 1C, insert). Its diameter is somewhat greater than the septin hourglass at the bud neck, which is brighter and wider. In typical experiments in which cells expressing GFP-Cdc3p are examined 2 hr after mixing, this structure is evident in >90% of zygotes for which plasma membrane fusion has occurred. Parental nuclei congress and fuse with each other when it is already in place (Figures 1B and 1C). The concentration of GFP-Cdc3 at the midzone is obvious for ~15 min. A patch of GFP-Cdc3p at the site of future bud emergence then appears (Figure 1C).

GFP-Myo1p is not detected at the cortex of the mating projection; however, it also forms an annulus in the midzone (Figure 1D). Judging from the distribution of GFP-tagged Act1p, and the actin-binding protein, Abp140/Trm140, and from staining fixed preparations with rhodamine-phalloidin, actin patches and cables are widespread but are not characteristically concentrated or oriented in the midzone at this time (see below).

Fluorescence recovery after photobleaching (FRAP) of GFP-Cdc3 in zygotes shows that the cortical collar, annulus, patch, and bud neck filaments are all dynamic. Because the estimates of half-time for recovery (13.5 ± 3.4 s to 27.1 ± 8.7 s, n = 5–21) and mobile fraction (28% ± 2.8% to 38% ± 8.5%, n = 5–21, SD) are relatively uniform among these structures, the successive redistribution of septins is likely to result from the progressive elimination and/or appearance of binding sites. Additional evidence of the dynamic nature of the annulus comes from fluorescence loss in photobleaching experiments: repeated photobleaching of the diffuse pool of GFP-Cdc3p in the zygote cytoplasm (avoiding the annulus itself) progressively weakens the signal in the annulus (Figure S1).

We therefore suggest the following sequence of septin morphogenetic intermediates (Figure 1E): (0) the collar of the mating projection, (1) the symmetric collar of early zygotes, (2) the annulus, (3) the patch at the site of bud formation, and (4) the bud neck itself. As explained below, these events are concurrent with changes in the actin cytoskeleton.

Because the medial concentration of septins becomes most obvious when parental nuclei establish contact, we explored the possibility that the annulus has a continuing association with the nucleus. In support of this possibility, we observe that (1) a narrowed segment of the nuclear envelope spans the midpoint of the zygote even after karyogamy and displacement of the chromatin mass to one side (Figure 1F), (2) nuclear pores are generally not detected at this point (Figure 1F), and (3) the annulus encircles the narrowed segment (Figure 1G).

Flux of Polysomes across the Midzone Is Delayed Relative to Soluble Tracers

Shortly after cell-cell contact is established, soluble DsRed (~120 kDa)—like GFP-Cdc3—suddenly redistributes from the donor to acceptor cell. Surprisingly, at this point, polysomes (including Rps3p-GFP or Rpl25p-mCherry) remain in their initial parental domain (Figure 2A). In fact, they begin to redistribute only when nuclei are about to establish contact—well after rupture of the plasma membrane—as judged by the apical elimination of the plasma membrane protein, Mid2p-GFP (Figures 2B–2D) that is present at the zone of contact prior to rupture. The equilibration of polysomes then requires ~10 min. The slow pace of these events suggests the presence of a barrier, given the apparent full disruption of the plasma membrane, the significant mobility of polysomes ($t_{1/2}$ for recovery after photobleaching ~16 s [Figure S2]), and electron micrographs that show a 0.5–1 micron gap between the nuclear envelope and the cortex of the zygote (Byers and Goetsch, 1975).

As illustrated above, while fluorescent polysomes gradually shift from *cis* to *trans*, there is a sharp discontinuity in their signal intensity. To learn whether the nucleus is responsible for this discontinuity and impedes transit through the midzone, we studied *kar1* × wild-type (WT) crosses, in which nuclei do not congress (Molk and Bloom, 2006) (Table 1). The presence of the nucleus at the midzone does not appear to contribute, because a sharp discontinuity in polysome distribution is evident in such crosses (Figure S3), and there is no significant acceleration of the rate of polysome redistribution in *kar1* × WT crosses in comparison to WT × WT crosses. Moreover, the redistribution of polysomes still precedes redistribution of the mitochondrial signal, as for WT × WT crosses (Figure S4).

Because septins concentrate at the zygote midzone, we also asked whether they contribute to the slow pace of flux. Indeed, a temperature increase from 23°C to 37°C causes a modest increase in the rate of flux in crosses between temperature-sensitive (ts) conditional septin mutants (*cdc12-6*), whereas no comparable increase is seen when WT control crosses are studied at the same temperatures (Table 1).

Flux of the Prion, Sup35 [*PSI+*], Is Delayed Relative to Sup35 [*psi*$^-$]

To learn whether Sup35p [*PSI*$^+$] readily traverses the midzone, we followed Sup35p-GFP in crosses in which one mating partner expresses a functional integrated copy of Sup35p-GFP from the *MFA1* promoter, which is turned off upon cell fusion. The same partner also expresses soluble DsRed or Rpl25-mCherry. In [*psi*$^-$] cells, cytoplasmic Sup35p-GFP is smoothly distributed and can diffuse freely, whereas the signal is generally inhomogeneous in [*PSI*$^+$] cells (Greene et al., 2009; Kawai-Noma et al., 2006; Satpute-Krishnan and Serio, 2005). In the "strong" [*PSI*$^+$] strains that we use, Sup35-GFP has a mottled/irregular appearance at steady state. The designation "strong" signifies that translation termination defects are suppressed more efficiently than by "weak" forms.

Redistribution of aggregated Sup35p-GFP in crosses between [*PSI*$^+$] cells is restricted at the midzone, judging from examination of intermediate time points (Figure 3A). This is reminiscent of previous studies of the [HET-s] prion (Mathur et al., 2012). The restriction is not simply due to the position of the nucleus, because an equivalent discontinuity is also evident in WT × *kar1* crosses in which the lack of karyogamy is ensured by following a marker of the endoplasmic reticulum (ER)/nuclear

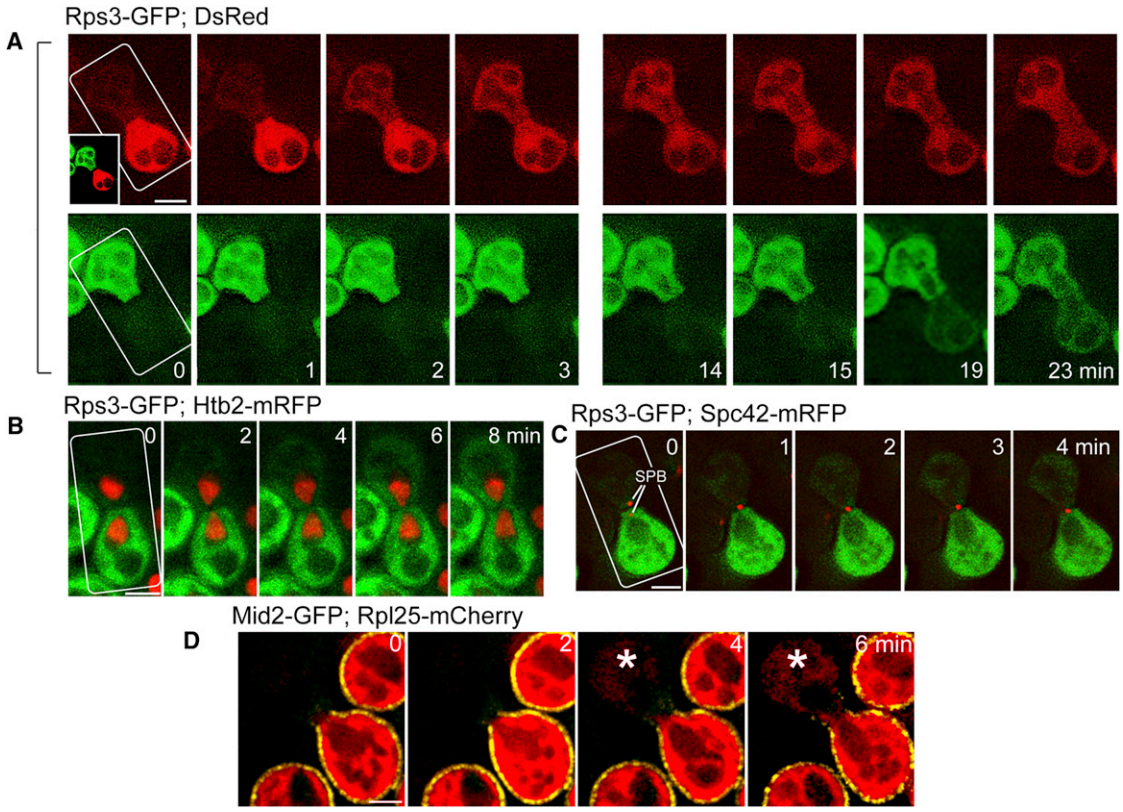

Figure 2. Redistribution of Polysomes

(A) Cytoplasmic DsRed transfers before polysomes. Time course of a cross between a strain expressing cytoplasmic DsRed (lower cell) and a strain expressing the tagged ribosomal protein, Rps3p-GFP (upper cell). Note that the flux of DsRed starts at the 0/1 min time point and that, by contrast, no transit of Rps3p-GFP is seen until after the 14 min time point. Rps3p-GFP is essentially entirely polysomal (Seiser et al., 2006). Rps3p-GFP was preinduced overnight. The two colors have been separated for clarity, while the insert in the first panel shows both signals. Strains: ATY3162 × ATY2872.

(B) Polysome transfer starts when nuclei are about to contact each other. Time course of a cross between a strain expressing Htb2p-mRFP (upper cell) and a strain expressing both Htb2p-mRFP and Rps3p-GFP (lower cell). Rps3p-GFP was preinduced overnight. Strains: ATY2835 × ATY3192.

(C) Polysome transfer starts as the spindle pole bodies (SPB) contact each other. Time course of a cross between a strain expressing both Rps3p-GFP and the tagged SPB protein, Spc42p-mRFP (lower cell), and a strain expressing Spc42p-mRFP (upper cell). The two SPBs contact each other at the 1 min time point and flux of Rps3p-GFP begins at this time. Strains: ATY1774 × ATY3190.

(D) Rupture of the plasma membrane does not initiate immediate flux of polysomes. Cross between a strain expressing the plasma membrane marker, Mid2p-GFP, and Rpl25p-mCherry-tagged polysomes (lower right) with an unlabeled strain (upper left). Note that although the plasma membrane is interrupted at t = 0, the flux of polysomal signal (*) is delayed and occurs only slowly. Strains: ATY2835 × ATY4252.

See also Figures S2, S3, and S4.

envelope (mRFP-HDEL) (Figure 3B). Moreover, in such crosses, redistribution of Sup35 still occurs before redistribution of mitochondria (not shown).

Further experiments help characterize the medial barrier and the in vivo hydrodynamic properties of Sup35p. First, Sup35p-GFP (91 kDa) [*psi*$^-$] and soluble DsRed (~120 kDa) have similar hydrodynamic properties in vivo: both transfer over the same period of time in crosses between [*psi*$^-$] cells (Figure 3C). Transfer of Sup35p-GFP is essentially complete before initiation of polysome equilibration (Figure 3D).

Moreover, progressive coalescence of diffuse Sup35p can be detected, possibly as a reflection of conformational maturation. Thus, when Sup35p-GFP from a [*psi*$^-$] "donor" enters a [*PSI*$^+$] "acceptor" environment, tiny just-discernable foci appear in the acceptor cell domain during the initial 30 min. At this resolution, these foci provide a first suggestion of conformational change and possible oligomer/aggregate formation. The donor cell domain, as in studies of heteroallelic conversion of the HET-s and HET-S proteins (Mathur et al., 2012), could receive nonfluorescent seeds of [*PSI*+] Sup35 in such experiments. We do not, however, see progressive changes in the donor compartment over the same period of time, perhaps because the size of any seeds precludes their rapid exchange (Figure 3Ea). More visible foci and extensive "mottling" do appear in both domains, but this occurs only gradually over 1–2 hr (e.g., Figures 3Eb and 3Ec). Curiously, an earlier study has described more rapid Sup35-GFP conversion during zygote formation (Satpute-Krishnan and Serio, 2005).

Furthermore, the overall polydispersity of Sup35p in a [*PSI*$^+$] environment appears comparable to that of polysomes; i.e., in [*PSI*$^+$] × [*PSI*$^+$] crosses in which both Sup35p-GFP and tagged polysomes are expressed by one parent, the transfer of

Table 1. Impact of Septin Mutants and Nuclear Congression on Polysome Flux

Strains		Slope at $t_{1/2}$ (%/min) 23°C	36°C
WT × WT	ATY4158 × ATY2871	5.4 ± 2.2 (n = 10)	4.6 ± 1.7 (n = 6)
cdc12-6 × *cdc12-6*	ATY4203 × ATY4223	5.1 ± 0.9 (n = 6)	10.4 ± 1.6 (n = 6)
kar1 × WT	ATY4187 × ATY1920	6.0 ± 2.2 (n = 13)	

Mixtures (MAT a, MAT α) of the indicated cells in log phase were spotted on an agar surface in growth medium. In each case, one partner expressed a tagged ribosomal protein. After 1.5 hr at 23°C, they were recovered and observed by DeltaVision microscopy at either 23°C or 36°C, as appropriate. Images were collected every 2 min through the period of *cis-trans* transfer of the fluorescent signal (~15 min). Image projections were deconvolved and pixel intensity was estimated at six to eight points in the cytoplasm per parental domain (Softworx). Average pixel intensity was then calculated. After curve fitting (Origin), the half-time for flux and corresponding slope (percent/min ± SD) were estimated. The increment of slope in the *cdc12-6* cross (37°C versus 23°C) has a p-value of < 0.05. *cdc12-6* was used for these experiments, because we have found that it is especially effective in causing septins at the bud neck to disperse at the restrictive temperature (data not shown). Flux of labeled polysomes also increased in *cdc11-6* crosses (3.2 ± 1.5 at 23°C versus 4.7 ± 2.6 at 36°C; n = 5–7); however, the increase was of marginal significance.

Sup35p-GFP aggregates extends over at least as long a period as for polysomes (Figure 3A).

Mitochondrial Encounters and Fusion

Progressive Sequestration of Septins to the Bud Neck Parallels Mitochondrial Encounters

After polysome and prion flux and completion of nuclear fusion, tagged mitochondria extend precisely up to the midzone, as though abutting on an invisible barrier (Figures 4A and 4B). During this period, however, their position is not further restricted—as in haploid cells, they can move extensively. Only after a 15–30 min delay do matrix markers contributed by one parent quickly access much of the mitochondrial labyrinth of the *trans* domain of the zygote (Figures 4A and 4B), presumably as a result of sudden fusion between the parental mitochondria (Hermann et al., 1998; Nunnari et al., 1997; Okamoto et al., 1998) (see also Figure S5). In Figure 4B, note that, prior to redistribution of the mitochondrial marker, a patch of GFP-Cdc3 appears at the site of bud formation (asterisk), as in Figure 1C. The consistency of this order is evident in experiments in which a parent that expresses GFP-Cdc3p was crossed with a parent that expresses the matrix marker, Cox4-DsRed: At a time point when redistribution of the matrix marker had occurred in half of the zygotes, a GFP-Cdc3-positive cortical patch or bud neck was evident in all zygotes (83/83).

The timing of redistribution of DsRed-Cox4 and the sequential morphogenesis of septin-containing structures suggests a "sequestration" hypothesis: The zygote midzone initially impedes encounter of parental mitochondria, the site of incipient budding then recruits components from the midzone (including septins), and the integrity of the midzone becomes so impaired that *cis-trans* encounter of parental mitochondria can occur. Relocation of selected proteins from the midzone to the bud neck could also cause secondary changes that promote redistribution, as is further discussed below.

Encounters of Mitochondria Require Actin Polymerization and Recruitment of Septins to the Bud Neck

To learn whether septin integrity affects encounter of parental mitochondria, we first evaluated redistribution of Cox4-DsRed in crosses between *cdc12-6* strains. These "two-step crosses" were initiated at 23°C and then reincubated for up to 40 min at 37°C versus 23°C. As shown in Figure 4C, redistribution is little affected at 37°C versus 23°C for the *cdc12-6* cross, and the rate is nearly identical at both temperatures for WT cells. In these experiments, multiple pools of septins are perturbed; i.e., any medial barrier could be weakened and any role for septins at the site of bud emergence could also be compromised.

We therefore studied redistribution of Cox4-DsRed in crosses of mutants that inhibit bud emergence (Figure 4C). In each case, one of the parents also expressed GFP-Cdc3p. Relevant mutants are *sec1-1*, an exocytosis ts mutant that stops budding (Togneri et al., 2006), and *cdc28-13*, the ts cyclin-dependent kinase mutant that stops both budding and deposition of septins at the site of bud formation in haploid cells (Cid et al., 2001). As expected, no zygotic buds formed in either cross at 37°C.

In *sec1-1* × *sec1-1* two-step crosses, a cortical patch of GFP-Cdc3p appeared in approximately two-thirds of zygotes within 40 min during the reincubation at 37°C, and the annulus became less evident with time (Figure 4D, left). Moreover, redistribution occurred at essentially the same rate at both 37°C and at 23°C (Figure 4Cd). The annulus is readily detected in *cdc28-13* × *cdc28-13* crosses, , but there was no cortical patch of GFP-Cdc3p after incubation at 37°C (Figure 4D, right). Moreover, the *cdc28-13* crosses consistently showed slower redistribution at 37°C than at 23°C (Figure 4Cc).

Parallel two-step crosses show that actin polymerization is required in order for redistribution of Cox4-DsRed, and addition of latrunculin A during the second incubation halts redistribution (Table 2). This treatment does not cause an obvious change in the distribution of GFP-Cdc3 (not shown).

Thus, encounter and fusion of parental mitochondria are delayed when the septin annulus is conspicuous and bud neck filaments have not formed. In this sense, by checking on the progress of bud formation, the timing of encounters between parental mitochondria is adjusted.

The Nucleus Impedes Redistribution

To learn whether the presence of the nucleus at the midzone delays the encounter of parental mitochondria, we evaluated redistribution of Cox4-DsRed in *kar1* × WT crosses, by comparison to WT × WT crosses, and observed that redistribution occurs earlier in the *kar1* × WT crosses (Figure 4Ce). Both septins and the nucleus thus contribute to the delay of mitochondrial encounter and fusion.

Entry into Buds

Sup35p [PSI$^+$] Enters All Buds

Some forms of Sup35p are not efficiently inherited during mitotic growth. Nevertheless, time-lapse observations of individual

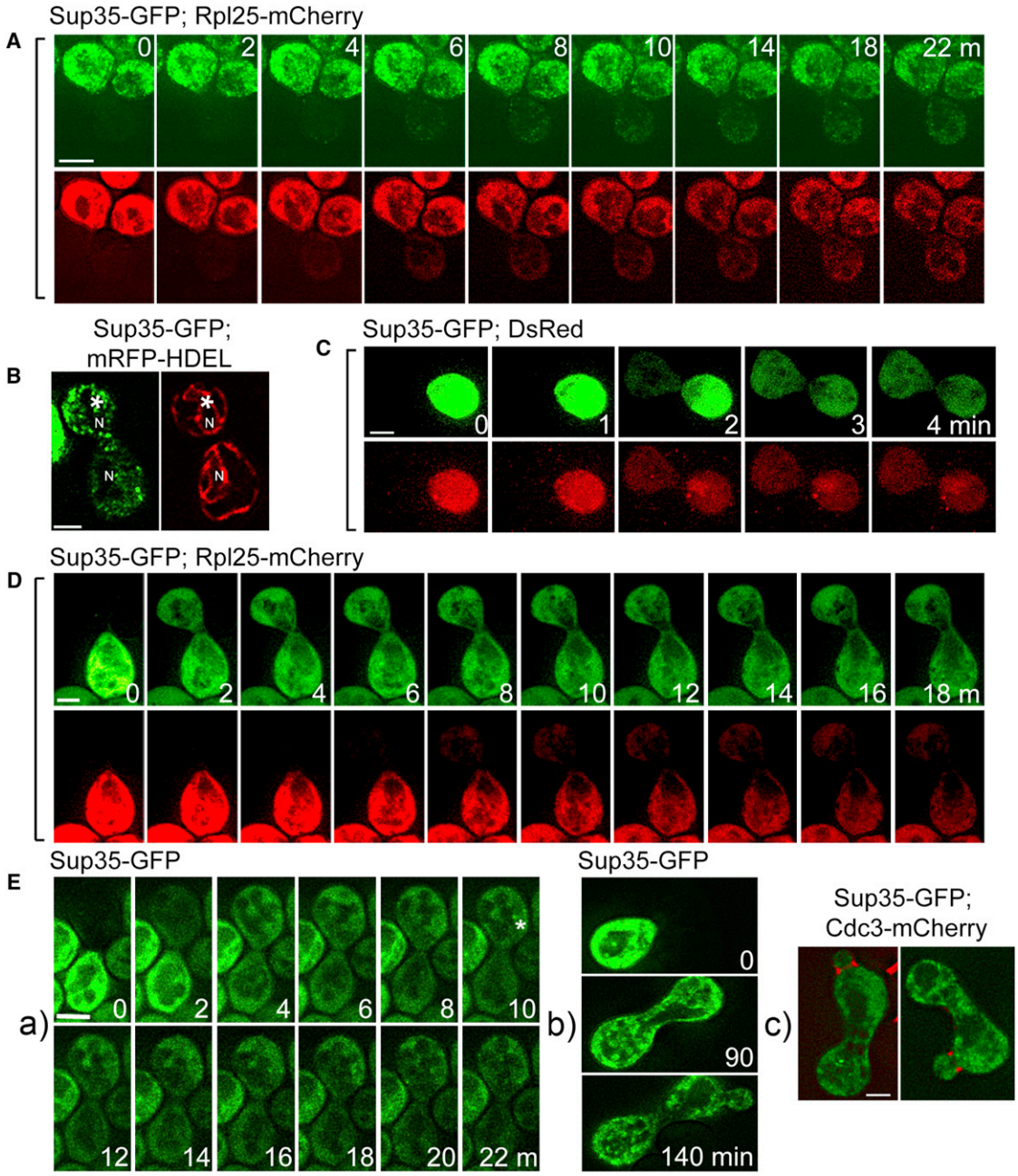

Figure 3. Redistribution of Sup35p-GFP

(A) Transit of Sup35p-GFP between [*PSI*$^+$] cells occurs concurrently with polysomes. Time course of a cross between a cell that expresses both Sup35p-GFP and Rpl25-mCherry (upper cell) and a nonfluorescent cell (lower cell). For Sup35p-GFP, note that although there can be initial transfer of very limited amounts of a diffuse pool (evident upon enlargement of the image), aggregates in the acceptor cannot be seen until the 4 min time point. Moreover, as for polysomes, there is a discontinuity of abundance of Sup35p-GFP aggregates at the midzone at intermediate time points. The slow transfer of Sup35p-GFP aggregates is concurrent with transfer of tagged polysomes. Strains: ATY4847 × ATY4519.

(B) Transit of Sup35p-GFP aggregates is restricted at the midpoint even when nuclei do not span the zygote midzone. The cross is between a [*PSI*$^+$] cell (upper cell) that expresses both Sup35p-GFP and the mRFP-HDEL luminal marker of the ER and nuclear envelope, with a *kar1* mutant (lower cell). An intermediate time point is illustrated. The visibility of the mRFP-HDEL throughout shows that the two cells have fused. Note that the nuclei have not fused and that the concentration of Sup35p-GFP aggregates (*) diminishes abruptly at the midpoint of the zygote. The two colors have been separated for clarity. N, nucleus. Strains: ATY3198 × ATY4826.

(C) Comparison of the rate of redistribution of Sup35p-GFP and DsRed. Both parents are [*psi*$^-$]. One expresses both Sup35p-GFP and cytoplasmic DsRed, whereas the other is not labeled. As shown, diffuse Sup35p-GFP (91 kDa) equilibrates over the same period of time as DsRed (120 kDa). Strains: ATY4901 × ATY4928.

(legend continued on next page)

[*PSI*$^+$] × [*PSI*$^+$] and [*PSI*$^+$] × [*psi*$^-$] zygotes in which aggregated Sup35p-GFP is introduced from a [*PSI*$^+$] parent show that all buds—including the smallest that are encircled by septins—receive aggregated Sup35p-GFP (e.g., Figures 3Eb and 3Ec), a process that is favored by fragmentation of prion units (Liebman and Chernoff, 2012; Paushkin et al., 1996). This is also true in [*psi*$^-$] × [*PSI*$^+$] crosses in which Sup35p-GFP is contributed by the [*psi*$^-$] parent. Indeed, there is no visible distinction between buds originating at the two distinct ends in [*psi*$^-$] × [*PSI*$^+$] crosses. Thus, although these aggregates of Sup35p^{strong}-GFP are delayed at the midzone, and although there can be quantitative differences in the relative abundance of aggregates among cells, they are transmitted to all progeny. It will be of interest to investigate the extent to which the [*RNQ*$^+$]/[*PIN*$^+$] status of cells and other forms of Sup35 (e.g., weak versus strong) influences transit between parental domains and entry into buds.

Nucleoids Enter Nascent Terminal Buds and Mother-Bud Continuity of Mitochondria Continues Until Telophase

To learn whether delayed fusion of parental mitochondria causes terminal buds to be enriched in a single parental mitochondrial genome, we conducted crosses in which one parent expressed tagged proteins of mitochondrial nucleoids—Abf2p-GFP or Mgm101p-GFP (Kucej et al., 2008; Meeusen et al., 1999; Okamoto et al., 1998)—and the other expressed Cox4-DsRed. Indeed, tagged nucleoid(s) consistently associate with adjacent nascent terminal buds well before *cis-trans* fusion of mitochondria (e.g., Figures 5A and S6).

The biased inheritance of mitochondrial genomes could signify that there is only a brief time window for association of mitochondria with terminal buds. Alternatively, mitochondria could retain continuity into the bud for an extended period of time, but nearby (*cis*) nucleoids that enter early might outnumber nucleoids derived from the distant parent, or associate with a finite number of binding sites. It is therefore important to learn for how long mitochondria remain continuous across the bud neck. Published images show continuity when buds are present (Boldogh et al., 2005; García-Rodríguez et al., 2009; Weisman, 2006).

Because buds form before entry of the nucleus, we have used two protocols to take this analysis a step further, showing that continuity of Cox4-GFP into buds continues when the nucleus spans the bud neck: (1) when the cell cycle is arrested by inactivating the mitotic exit network kinase, Dbf2p (Figure 5B), and (2) after depletion of the activator of the anaphase promoting complex, Cdc20p (Komarnitsky et al., 1998) (Figure 5C). In the latter case, we have used FRAP to assess functional continuity. When the bud is bleached, the signal can (1) diminish in the bud but not change in the zygote, (2) immediately diminish in both bud and in the zygote, or (3) recover in the bud only after a delay. Each outcome is observed with comparable frequency. Thus, although mother-bud continuity can be intermittent, it persists until after entry of the nucleus.

Mitochondria Enter Medial Buds before Fusing

Both parental types of mitochondria are present in most diploid cells that originate from medial buds, although one type is lost (at random) within a few generations (Birky et al., 1978; Dujon et al., 1974; Okamoto et al., 1998; Thomas and Wilkie, 1968). Because there has been no indication of whether parental mitochondria fuse with each other before entry into buds, we have studied early stages of medial bud emergence using parents that express Cox4-DsRed versus Cox4-GFP. One readily finds examples in which both types of mitochondria extend to the bud neck but have not fused, suggesting that the two types of parental mitochondria generally fuse with each when they enter the bud (Figure 5D). Thus, as for nonmedial events, fusion occurs when bud formation is already underway. Interestingly, fusion of parental vacuoles also does not occur before entry into medial buds (Weisman, 2006).

The Septin Ring at the Bud Neck Is Required for Actin Polarization

Why do parental mitochondria not fuse with each other long before bud formation? Is a medial barrier strongly restrictive, or do bud formation, the arrival of septins at the neck, and actin polarization also have a positive effect? To explore this issue, we first localized mitochondria along with actin cables by following Cox4-DsRed and a GFP-tagged copy of the actin filament-binding protein, Abp140 (Yang and Pon, 2002) (Figure 5E). Prior to cell-cell fusion, actin cables and mitochondria orient toward the zone of contact. Upon fusion, actin orientation becomes less obvious, the midzone often appears depleted of filaments, and, as detailed above, mitochondria extend only to the midpoint of the zygote. When buds become visible, actin has reorganized to generate cables that extend from the bud neck and extend either in roughly symmetric fashion toward each parental domain (when budding is medial), or along the long axis of the zygote (when budding is nonmedial). In each case, mitochondria appear to align with cables.

In mitotic cells, septins and the formin Bnr1p localize to the bud neck and are required for nucleating linear actin filaments in the mother cell. A second formin, Bni1p, localizes to the bud tip and plays a similar role for organization of actin in the bud (Buttery et al., 2007; Pruyne et al., 2004). We therefore investigated the interdependence of septin localization, Bnr1p, and actin polarization in zygotes.

(D) Transit of Sup35p-GFP precedes polysomes in crosses of [*psi*$^-$] cells. One parent expresses both Sup35p-GFP and Rpl25p-mCherry (lower cell), whereas the other is unlabeled. Note that Sup35p-GFP enters the acceptor well before polysomes. Strains: ATY4848 × ATY4928.

(E) Entry of diffuse Sup35p-GFP from a [*psi*$^-$] cell into a [*PSI*$^+$] environment leads to its slow aggregation. In all cases, [*psi*$^-$] cells expressing Sup35p-GFP were crossed with [*PSI*$^+$] cells. (a) When Sup35p-GFP (lower cell) enters the [*PSI*$^+$] cell (upper cell), fine foci form during the first 20–30 min, especially in the acceptor cell cytoplasm. In this case, the first aggregates are seen at the 10 min point (*). Strains: ATY4841 × ATY4519. (b) In a parallel experiment, the incubations extended for longer, and obvious extensive aggregation/mottling was seen throughout. In this cross, the acceptor strain included a fluorescent reporter (pRS304-P_{GPD}GST [UGA]DsRed) to verify the [*PSI*$^+$] status of the environment (Satpute-Krishnan and Serio, 2005). Strains: ATY4841 × ATY4973. (c) Crosses of the Sup35p-GFP-expressing strain with a strain that expresses Cdc3p-mCherry show that even small zygotic buds receive Sup35p-GFP [*PSI*+] aggregates, and that, as for haploid and diploid buds, the zygotic bud neck is encircled by septins. Strains: ATY4840 × ATY5457.

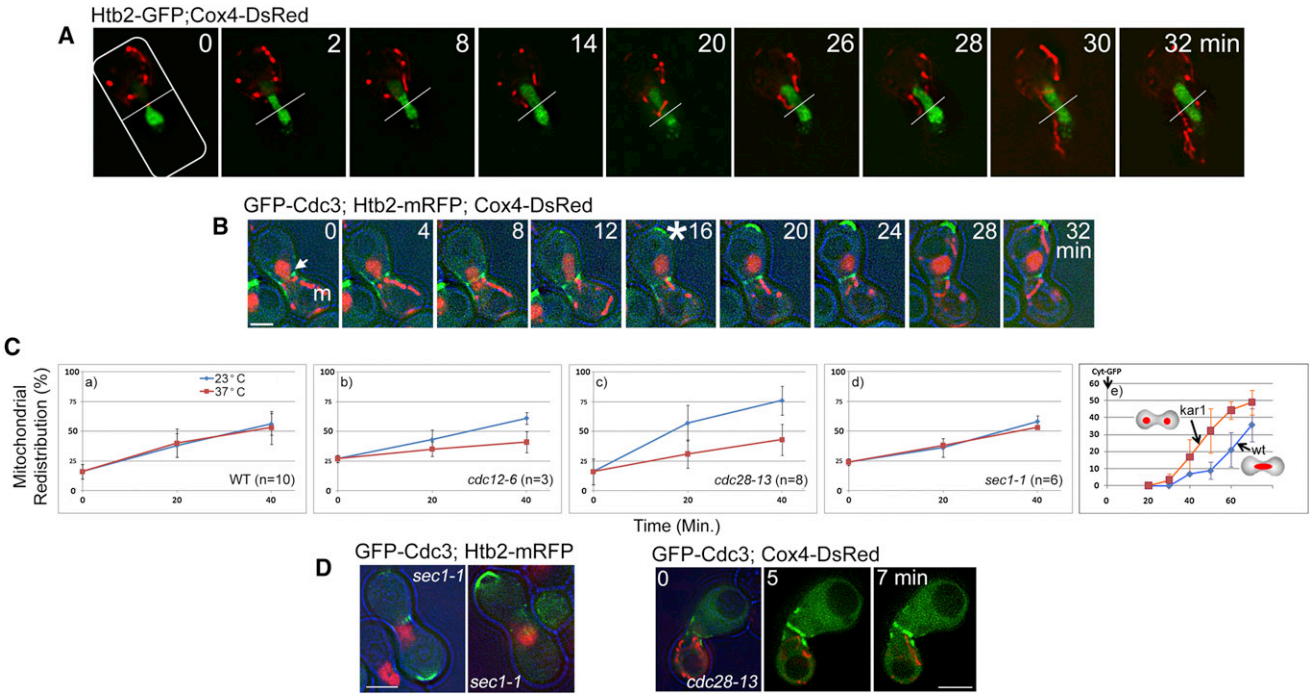

Figure 4. Encounter of Mitochondria

(A) Karyogamy precedes transfer of the mitochondrial signal. Time course of a cross between a strain that expresses Htb2p-GFP (lower cell) and a strain that expresses the mitochondrial matrix marker, Cox4-DsRed (upper cell). Karyogamy is indicated by the increase in nuclear volume between the 0 and 2 min time points. The distribution of red mitochondria appears to be limited by an invisible barrier (white line). Karyogamy precedes the sudden arrival of the red mitochondrial signal in the *trans* cell (between the 28 and 30 min time points). Strains: ATY2707 × ATY2673.

(B) Timing of mitochondrial encounters compared to septin morphogenesis. Time course of a cross between a strain expressing GFP-Cdc3p and Htb2p-mRFP (left) and a strain expressing Cox4-DsRed (right). Note that the red mitochondria (m) from the lower right abut on the septin annulus (arrow) at early time points. The site of incipient bud formation then develops a patch of GFP-Cdc3p (* at 16 min). When the site of budding is well defined (28 min), the red mitochondrial signal suddenly enters the upper volume of the zygote. Strains: ATY3432 × ATY3129.

(C) Quantitation of redistribution of mitochondrial proteins. All panels concern crosses in which one partner expresses Cox4-DsRed. For (a)–(d), pairs of wild-type (a), *cdc12-6* (b), *cdc28-13* (c), or *sec1-1* (d) strains were crossed for 1.5 hr on plates, recovered (t_o), and then incubated at 23°C or 37°C for the indicated times before fixation and quantitation to determine the percent of zygotes for which Cox4-DsRed extended into both parental domains. The values at t_o do not start from 0% because the initial incubation inevitably already allows limited redistribution. As expected, the *sec1-1* and *cdc28-13* zygotes did not bud at 37°C. Note that the temperature increase has little effect on the speed of Cox4-DsRed redistribution in WT, *sec1-1*, and *cdc12-6* crosses. The effect on *cdc28-13* crosses is more distinct. (Because the parent of this mutant was not available, the temperature dependence of redistribution should be noted, rather than comparison to rates of redistribution in a.) Redistribution accelerates when the nucleus is absent from the midzone (e). In this case, a WT × WT cross and a *kar1* × WT cross were compared. One parent expressed cytoplasmic GFP to estimate its time of permeation. In both cases, the flux of cytoplasmic GFP was designated t_0. Note that the half-time for redistribution of the mitochondrial signal is advanced by about 20 min in the *kar1* cross, relative to WT. For (a)–(e), 200 zygotes were counted for each of three to ten experiments. Data are expressed as means ± SD. For (b) and (c), the differences between the final data points have a p value of < 0.1 (Student's t test). For (e), the p-values between the data points for the two lines range from 0.05 to 0.1 (Student's t test). Strains: (a) ATY2707 × ATY2112, ATY4054 × ATY4059, and ATY4250 × ATY4291; (b) ATY3459 × ATY4028; (c) ATY4051 × ATY2773; (d) ATY4052 × ATY4058; (e) ATY2869 × ATY3129 and ATY2869 × ATY4017. Because the parent of the *cdc28-13* strains was not available, the WT data that are compared to *cdc28-13* illustrate an average from several parental strains.

(D) Localization of GFP-Cdc3p after arrest. Left two panels show an isogenic pair of *sec1-1* strains crossed at 23°C. One expressed Htb2p-mRFP, while the other expressed GFP-Cdc3p. After 1.5 hr, they were reincubated 40 min at 37°C. As shown, zygotes accumulate GFP-Cdc3p at the site of imminent bud formation. *sec1-1* does not block nuclear fusion (Tartakoff and Jaiswal, 2009). Strains: ATY4031 × ATY3842. Right three panels show an isogenic pair of *cdc28-13* strains crossed at 23°C. One expressed Cox4-DsRed, while the other expressed GFP-Cdc3p. After 1.5 hr, they were reincubated at 37°C for 40 min. Note the conspicuous annulus and the lack of redistribution of the mitochondrial signal. In parallel WT crosses, 40 min is sufficient to allow redistribution of mitochondrial proteins in the large majority of zygotes. Strains: ATY3773 × ATY2773.

See also Figure S5.

In crosses between WT cells, we observe that GFP-tagged Bnr1p becomes visible only when zygotic buds emerge; i.e., approximately when actin becomes repolarized and parental mitochondria fuse. At this time, it colocalizes with septins at the bud neck (Figure 5F).

To learn whether septins at the bud neck are required for colocalization of Bnr1p and for actin polarization throughout the zygote, we allowed bud formation to begin and then inactivated one septin at the bud neck. In these experiments, we formed *cdc11-6* zygotes at 23°C, using a pair of temperature-sensitive strains that express mCherry-tagged Cdc3p and GFP-tagged Bnr1p. When the zygotes were then shifted to 36°C–37°C, both tagged Cdc3p and tagged Bnr1p disappeared from the bud neck (Figure 5G, panel 1). Moreover, in equivalent protocols

Table 2. Impact of Latrunculin A on Redistribution of Mitochondria

	% Redistribution			
Experiment	t_0	+60 min	+60 min with LTA	% Inhibition
1	27 ± 7.2	63.3 ± 3.8	29.7 ± 2.5	94%
2	27.5 ± 3.5	73 ± 4.2	37.5 ± 3.5	77%
3	43.7 ± 4.0	65.7 ± 3.2	40.5 ± 3.5	100%

One parent expressed soluble GFP in the cytoplasm, whereas the other expressed Cox4-DsRed. Typical crosses were harvested when cell fusion was first detected (t_0). At this point, redistribution of the Cox4-DsRed had occurred in 27%–43% of the zygotes that already showed flux of cytoplasmic GFP. The samples were then diluted 5× and reincubated for 1 hr in growth medium ± 15 μM latrunculin A before fixation. DMSO 1% was present in all samples. For each condition, 400–600 zygotes showing flux of cytoplasmic GFP were scored according to whether Cox4-DsRed was evident in both parental lobes. The percentage that showed redistribution was expressed as an average ± SD. Three representative experiments are tabulated. Strains: ATY4697 × ATY3817. LTA, latrunculin A.

in which one of the haploid parents expressed tagged Abp140, actin cables became dramatically concentrated in the elongated buds and remarkably absent from the rest of the zygote (Figure 5G, panels 2–4). No such changes occurred in parallel experiments with WT zygotes. Because *bnr1Δ* strains do not form conventional zygotes with good efficiency, it has not been possible to inquire whether Bnr1p itself is needed (unpublished data).

There is thus a close connection between arrival of septins at the bud neck and the polarization of actin in the body of the zygote. We propose that this repolarization of actin facilitates fusion of parental mitochondria in zygotes.

DISCUSSION

The Importance of the Midzone

The ultimate redistribution of parental constituents during zygote formation occurs asynchronously (Figure 6A). Why is this? During the mitotic cell cycle, septin filaments that encircle the bud neck contribute to the restricted diffusion of cortical proteins between mother and bud. The present observations indicate that septin-containing structures serve a broader "gatekeeper" function, in that they can also control the flux of entities that are not primarily associated with the cortex. Polysomes and Sup35-GFP [*PSI+*], as well as mitochondria, are delayed at the level of the zygote midzone, which includes a septin annulus. Subcompartmentalization of the cytoplasm in the absence of membrane barriers is in fact characteristic of many cell types (Caudron and Barral, 2009; Galiano et al., 2012; Kissel et al., 2005; Lin et al., 2009; Merisko et al., 1986; Mollenhauer and Morré, 1978; Song et al., 2009; Wolosewick and Porter, 1979).

Interestingly, the septin annulus continues to encircle the nucleus well after karyogamy, and one report concludes that septins at the bud neck restrict transit of nuclear pores into buds (Shcheprova et al., 2008). Therefore, the efficacy of the midzone barrier could be promoted by its association with both the nuclear envelope and the plasma membrane, perhaps due to binding of septins to phosphoinositides (Casamayor and Snyder, 2003). Nevertheless, constriction around the nucleus does not account for all barrier function of the midzone: significant delay in redistribution persists even when nuclei do not congress. The functional significance of this barrier could normally be to buffer motion and thereby promote the surely intricate multistep process by which nuclei fuse (Melloy et al., 2007; Tartakoff and Jaiswal, 2009). Further interesting possibilities are that the populations of ribonucleoproteins on either side of the midzone are distinct and that, given the restricted transit of Sup35 [*PSI+*], the fidelity of translation termination is different within different parts of the cytoplasm.

Encounters of Parental Mitochondria

Parental mitochondria contact each other and fuse long after the flux of polysomes and Sup35p-GFP. What causes this delay? Fusion is linked to relocalization of septins to the bud neck and polarization of the actin cytoskeleton. Most strikingly, in septin mutant zygotes, at the restrictive temperature, actin cables vanish from the body of the zygote and become dramatically concentrated in emerging buds. The present observations thus strongly reinforce the concept that septins coordinate the organization of other components of the cytoskeleton (Kusch et al., 2002; Pruyne et al., 2004; Spiliotis and Gladfelter, 2012). Moreover, the rearrangement of actin filaments that occurs in septin mutants is likely to contribute to their inability to accomplish cytokinesis (Hartwell, 1971).

We suggest that slight translocation of both types of parental mitochondria across the midzone is normally required for their encounter, and that this step requires reorganization of the actin cytoskeleton. Concurrent remodeling of the midzone—including removal of septins—may facilitate these encounters.

Prior to cell fusion, actin cables in parental cells run antiparallel relative to each other (Slaughter et al., 2009) (Figure 6B). After cell fusion, cables in the body of the zygote have a less defined orientation until they extend either from the neck of medial buds into each parental domain, or from the neck of lateral or terminal buds along the full length of the zygote. In both situations, the actin filament nucleator, Bnr1p, localizes to the bud neck. Judging from our observations, mitochondrial fusion occurs in the middle of the zygote in both situations. This could signify that parallel alignment of linear actin filaments is required for in vivo mitochondrial fusion to occur.

We therefore suggest that several parameters determine which mitochondrial genomes are inherited by terminal buds. These include the timing of alleviation of the medial impasse and the timing of repolarization of the actin cytoskeleton. Because the progressive sequestration of septins away from the midzone to the bud neck couples these events, encounter and fusion of parental mitochondria is expected to be delayed but efficient. Further considerations also oppose entry of *cis* nucleoids into *trans* buds: (1) nucleoids are tethered to transmembrane proteins (Boldogh and Pon, 2007), and (2) nucleoids would likely encounter significant difficulty if they were to enter the *trans* mitochondrial reticulum of tubules after *cis-trans* fusion and then need to pass beyond nucleoids of the other parent to gain access to the bud.

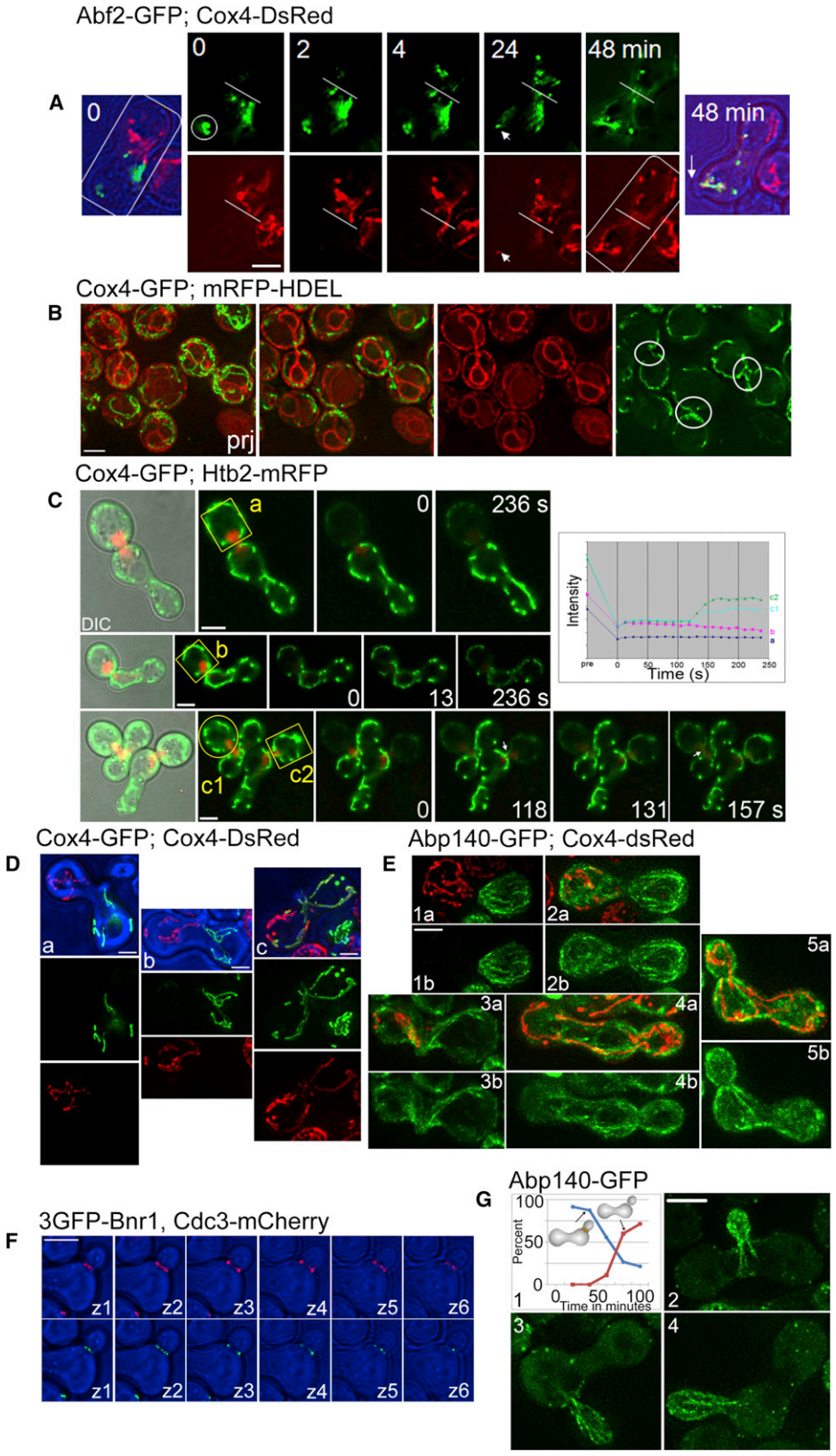

(legend on next page)

Generality

The uniparental inheritance of mitochondria that is characteristic of many organisms suggests that there is an advantage to protecting at least some copies of the mitochondrial genome from recombination. Alternatively, mitochondrial-nuclear interactions could become deleterious in the presence of more than one mitochondrial genome (Birky, 2001; Lewontin, 1971), or consequences of possible genetic incompatibilities could become manifest (Saupe, 2011). Interestingly, several conditions affect both the inheritance of mitochondria in humans (Dimauro and Davidzon, 2005) and the segregation of distinct mitochondrial genomes when they coexist (Jokinen and Battersby, 2012). Moreover, septin integrity is critical for proper differentiation of spermatozoa and compartmentalization of their mitochondria (Ihara et al., 2005; Kissel et al., 2005; Lin et al., 2009), and cell polarity defects and formin mutations have been linked to several diseases (DeWard et al., 2010; Stein et al., 2002).

Spatially separate cytoplasmic characteristics of cells can be differentially passed to daughter cells if the ends of the mitotic spindle extend into these distinct regions. For such a mechanism to function, the underlying characteristics could either be locally tethered (Spokoini et al., 2012) or restricted by barriers.

EXPERIMENTAL PROCEDURES

Cells, Plasmids, and Drugs

Yeast strains were primarily derivatives of W303 or S288C (Table S1). Table S2 lists yeast plasmids. Cells were grown in complete synthetic medium or appropriate drop-out media at room temperature, supplemented with adenine sulfate. As needed, cells were precultured overnight, or induced for 1–2 hr, in medium supplemented with 1% galactose and 1% raffinose, as indicated in the figure legends. All chemicals were from Sigma-Aldrich, except for latrunculin, which was from Millipore. Drug stocks (100×) were prepared in DMSO.

Protocols to Generate Zygotes

Strains (MAT a, MAT α) grown to OD_{600} ~2 were diluted 20× in medium and allowed to regrow with shaking for 2–3 hr before mixing equal numbers of appropriate pairs at OD ~4 in fresh medium. Then, 50–100 μl samples were applied to the surface of CSM-glucose plates at 23°C. When the

Figure 5. Entry into Buds

(A) Nucleoids enter the bud before *cis-trans* mitochondrial fusion. A strain expressing the tagged nucleoid protein, Abf2p-GFP (lower cell), was crossed with a strain expressing Cox4-DsRed (upper cell). The first and last panels include bright-field images to show that labeled nucleoids are adjacent to the bud even at t = 0, well before Cox4-DsRed redistributes. In experiments in which the bud emerges from the end of the zygote that expresses Cox4-DsRed, this marker enters buds well before *cis-trans* transit of Abf2p-GFP. Strains: ATY3576 × ATY3129.

(B) Mitochondria extend across the neck until after entry of nuclei into the bud. A MEN mutant (*dbf2-2*) that expresses both mRFP-HDEL and Cox4-GFP was incubated for 3 hr at 37°C and examined at 37°C. In cells in which the nucleus spans the bud neck (proving that bud formation is advanced but cytokinesis has not occurred), mitochondria can be traced from mother to daughter in most cells. The first panel (prj) is a projection showing both signals, whereas the second through fourth panels are single planes showing that both the nuclear envelope and mitochondria extend across the neck (white circles). Equivalent observations have been made with zygotes. Strain: ATY4818.

(C) Photobleaching assessment of mitochondrial continuity upon arrest of the cell cycle by depleting Cdc20p in zygotes. Two strains were crossed in methionine-free medium for 2 hr. Each had been engineered to allow depletion of Cdc20p upon transfer to methionine-containing medium, and each expressed both Htb2p-mRFP and Cox4-GFP. The mating mixture was then transferred to methionine-containing medium for 4 hr and used for photobleaching. Zygotes were selected for which the nucleus (red) spanned the bud neck. After photobleaching the buds, images were collected to follow GFP fluorescence in the bud and in the body of the zygote. The graph indicates three distinct behaviors: (a, upper) lack of recovery in the bud and lack of change in the zygote, (b, middle) instant recovery of the bud and unchanged intensity in the zygote, and (c and c′, lower) initial bleaching of the bud followed by delayed recovery in two zygotes. Each behavior was seen with roughly equal frequency. Strains: ATY4672 × ATY4698.

(D) Entry of mitochondria into medial buds. To monitor the relative position of the two parental populations of mitochondria, crosses between cells expressing Cox4-GFP and cells expressing Cox4-DsRed were examined. Projections are illustrated in which individual colors have been separated. In the example at the left (a), only one type of mitochondrion (green) extended into the bud. In the example in the middle (b), both types of mitochondria contacted the base of the bud, but had not fused. In the example at the right (c), fusion had occurred. Brightfield images are in blue. Strains: ATY2707 × ATY2708.

(E) Localization of actin cables during zygote formation. Cells expressing the GFP-tagged actin-binding protein, Abp140, were crossed with cells expressing Cox4-DsRed. Projections of 0.1 μ sections are illustrated. Note that prior to cell fusion (1a/b), actin cables and mitochondria polarize toward the zone of contact. After fusion, the polarity of actin is less clear (2a/b); however, as buds appear, cables are evident, some of which are oriented toward the bud. Both for medial and for nonmedial budding, mitochondria appear to associate with a subset of the cables (3–5a/b). In each pair of images, we illustrate the Abp140-GFP signal with (a) and without (b) the mitochondrial signal. Strains: ATY3072 × ATY3129.

(F) Distribution of the formin-like protein, Bnr1p-GFP, in zygotes. A strain expressing functional GFP-tagged Bnr1p was crossed with a strain expressing Cdc3p-mCherry. No GFP signal was seen in prezygotes or early zygotes, although GFP-tagged versions of other proteins involved in actin guidance (e.g., Abp1p, Bni1p, Bud6p) do concentrate at the zone of contact just prior to cell fusion (not shown). When buds emerge (either medial or nonmedial), foci of Bnr1p-GFP overlap the septin signal at the bud neck. A through-focal series (0.5μ per section) is illustrated, showing half of a zygote that bears a terminal bud. The two colors: red (upper) and green (lower) have been separated for clarity. Strains: ATY5527 × ATY5471.

(G) Control of actin polarization. (1) Localization of Bnr1p upon inactivation of Cdc11. A pair of *cdc11-6* strains expressing GFP-tagged Bnr1p or Cdc3p-mCherry was crossed at 23°C until zygotes formed and budding was evident. At this time, tagged Bnr1p and Cdc3p were visible at the bud neck of >90% of all zygotes. The preparation was then maintained at 23°C or shifted to 37°C to evaluate the signal at the bud neck (percent). As indicated in the graph for zygotes at 36°C–37°C, the proportion of budded zygotes showing both signals at the neck (blue line) progressively diminished, while the percent lacking both signals (red line) increased. At intermediate times, a minority of zygotes was found in which only Cdc3-mCherry was still detected at the neck. Upon incubation at 23°C over the same period, both labels persisted at the neck (not shown). Strains: ATY5535 × ATY5529. (2–4) Actin cables reorganize upon inactivation of Cdc11. A *cdc11-6* strain expressing GFP-tagged Abp140 was crossed at 23°C with a *cdc11-6* strain expressing Cdc3p-mCherry. When buds appeared, the preparations were shifted to 36°C–37°C for 90 min and then imaged. Representative projections are shown for cells in which Cdc3-mCherry can no longer be detected. Note the accentuated cables in the buds, cables that extend from buds into the body of the zygote, and the nearly complete disappearance of filaments from the rest of the zygote. WT zygotes do not show such relocalization of Abp140 in parallel experiments. Strains: ATY5539 × ATY5529.

See also Figure S6.

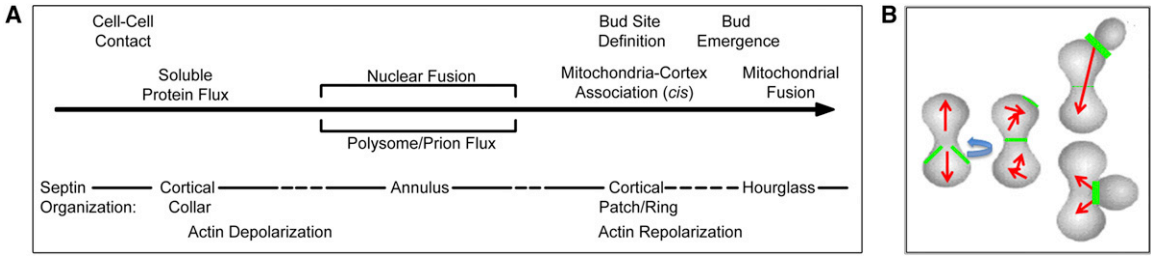

Figure 6. Overview

(A) Timeline. From top-to-bottom, the rows outline (1) sequential changes at the cell surface; (2) the redistribution of tagged soluble proteins, polysomes, aggregated Sup35 and mitochondria; (3) changes in septin organization; and (4) changes in actin polarization. The designation (*cis*) signifies that mitochondria contact the cortex at one end of the zygote where buds will subsequently form. The timing of fusion of parental mitochondria overlaps with the first signs of bud emergence per se. There is considerable polydispersity in the timing of these events. In general, upon mixing the two cell types at room temperature on the surface of an agar plate, zygotes first become visible after 1.5–2 hr. Soluble proteins then redistribute within ~20 min, polysome flux and nuclear fusion follow over ~20 min, and parental mitochondria fuse ~20 min later. Under the circumstances studied, the majority of buds emerge at terminae of the zygote.

(B) Model of actin polarization. The red arrows indicate the suggested direction of polarization, with the tail of the arrows corresponding to the site of nucleation. At the right, nonmedial (upper) and medial (lower) budding options are diagrammed. Green designates septins, as in Figure 1E.

samples had dried (~15 min), the plates were covered and incubated for 1.5–2.0 hr to generate early, unbudded zygotes. To quantitate redistribution of mitochondria (Cox4-DsRed), samples washed off plates were either fixed at once or first reincubated at OD_{600} = 1 in appropriate medium at 23°C or 37°C. For fixation, an equal volume of 4% formaldehyde in PBS was added on ice. After 5 min, the samples were washed with water and examined by epifluorescence.

Zygotes that were sufficiently mature to have a smooth concave contour at the middle and lacking any demarcation of the midpoint were scored in blinded fashion according to whether the mitochondrial marker was confined to a single parental domain. In selected experiments (see text), one partner expressed cytoplasmic GFP so that attention could be restricted to those zygotes for which the GFP was certain to have equilibrated. In fact, equilibration was seen in >85% of zygotes, as identified by strictly anatomic criteria.

Microscopy

For time-lapse microscopy of zygotes, samples of mating mixtures were rinsed off plates with complete medium at the indicated times and sedimented. Samples of the pellet (1 μl) were applied to 1.5% agarose pads including medium and additives of interest. After overlaying a coverslip and sealing with Vaseline, they were examined by DeltaVision microscopy at 23°C (unless specified otherwise).

For DeltaVision microscopy, we used a 100× oil immersion objective without binning (Olympus UPlanApo 100×/1.40; ∞/0.17/FN26.5). z stacks were deconvolved using Softworx and processed minimally. At least 20 cells were observed for each condition and the selected illustrations are representative of the large majority (>80%). Brightfield images are in blue. Successive z-planes were generally collected at 0.2–0.4 μ intervals and complete through-focal series were examined in all cases. Images were collected at 15 s to 30 min intervals, as appropriate. For most experiments, single planes are illustrated to optimize resolution. Other relevant information was not evident in alternative planes or in projections. Any use of entire z stack projections is specified in the legends.

To visualize actin, cells were fixed 10 min in ice-cold 70% ethanol, washed in PBS, stained for 2 min at room temperature with 0.14 μM rhodamine-phalloidin (Sigma 77418), washed repeatedly with PBS, and examined.

Photobleaching was performed with a Zeiss 510 confocal microscope using a Plan-Apochromat 100× oil-immersion objective (NA 1.4). After bleaching ~80% of the signal at 50% laser intensity, cells were imaged at 1% laser intensity using the acquisition software LSM510 (Carl Zeiss MicroImaging). When transformants that express Cox4-DsRed (ATY3129) were entirely photobleached and then followed over the next hour at room temperature, only minimal recovery of signal was seen (data not shown). Therefore, the contribution of new synthesis of Cox4-DsRed is equally minor over this period of time.

Quantitation and Statistics

All quantitative experiments are expressed as mean ± SD. P values were calculated using Student's t tests. The illustrated time-lapse series are representative of at least 20 independent cells or zygotes.

SUPPLEMENTAL INFORMATION

Supplemental Information includes six figures and two tables and can be found with this article online at http://dx.doi.org/10.1016/j.celrep.2012.11.022.

LICENSING INFORMATION

ACKNOWLEDGMENTS

We thank Dr. D. McDonald for use of microscopic facilities and A. Camacho, V. Cheruvu, A. Feczko, C. Hollegien, M. Khan, M. Lam, M. Mattera, F. Najm, C.-L. Ni, R. Patel, S. Rinonos, S. Roy, J. Toska, and Y. Zhang for help with experiments. Thanks to the following for materials: Y. Barral, E. Bi, R. Davis, V. Doye, S. Emr, P.-E. Gleizes, E. Grote, W. Huh, A. Johnson, R. Jensen, M. Kucej, S. Liebman, P. Novick, J. Nunnari, E. O'Shea, D. Pellman, E. Pon, M. Rose, R. Rothstein, K. Runge, and T. Serio. Thanks to D. Goldfarb and K. Weis, and to the anonymous reviewers for comments on the manuscript. This work was supported by NIH grants P30 CA43703-12 and R01GM089872.

Received: June 23, 2012
Revised: September 27, 2012
Accepted: November 27, 2012
Published: December 27, 2012

REFERENCES

Aguilaniu, H., Gustafsson, L., Rigoulet, M., and Nyström, T. (2003). Asymmetric inheritance of oxidatively damaged proteins during cytokinesis. Science *299*, 1751–1753.

Bagriantsev, S.N., Gracheva, E.O., Richmond, J.E., and Liebman, S.W. (2008). Variant-specific [PSI+] infection is transmitted by Sup35 polymers within [PSI+] aggregates with heterogeneous protein composition. Mol. Biol. Cell *19*, 2433–2443.

Balasubramanian, M.K., Bi, E., and Glotzer, M. (2004). Comparative analysis of cytokinesis in budding yeast, fission yeast and animal cells. Curr. Biol. *14*, R806–R818.

Barral, Y., and Liakopoulos, D. (2009). Role of spindle asymmetry in cellular dynamics. Int. Rev. Cell Mol. Biol. *278*, 149–213.

Bi, E., Maddox, P., Lew, D.J., Salmon, E.D., McMillan, J.N., Yeh, E., and Pringle, J.R. (1998). Involvement of an actomyosin contractile ring in Saccharomyces cerevisiae cytokinesis. J. Cell Biol. *142*, 1301–1312.

Birky, C.W., Jr. (1975). Zygote heterogeneity and uniparental inheritance of mitochondrial genes in yeast. Mol. Gen. Genet. *141*, 41–58.

Birky, C.W., Jr. (2001). The inheritance of genes in mitochondria and chloroplasts: laws, mechanisms, and models. Annu. Rev. Genet. *35*, 125–148.

Birky, C.W., Jr., Demko, C.A., Perlman, P.S., and Strausberg, R. (1978). Uniparental inheritance of mitochondrial genes in yeast: dependence on input bias of mitochondrial DNA and preliminary investigations of the mechanism. Genetics *89*, 615–651.

Boldogh, I.R., and Pon, L.A. (2007). Mitochondria on the move. Trends Cell Biol. *17*, 502–510.

Boldogh, I.R., Fehrenbacher, K.L., Yang, H.C., and Pon, L.A. (2005). Mitochondrial movement and inheritance in budding yeast. Gene *354*, 28–36.

Buttery, S.M., Yoshida, S., and Pellman, D. (2007). Yeast formins Bni1 and Bnr1 utilize different modes of cortical interaction during the assembly of actin cables. Mol. Biol. Cell *18*, 1826–1838.

Byers, B., and Goetsch, L. (1975). Behavior of spindles and spindle plaques in the cell cycle and conjugation of Saccharomyces cerevisiae. J. Bacteriol. *124*, 511–523.

Casamayor, A., and Snyder, M. (2003). Molecular dissection of a yeast septin: distinct domains are required for septin interaction, localization, and function. Mol. Cell. Biol. *23*, 2762–2777.

Caudron, F., and Barral, Y. (2009). Septins and the lateral compartmentalization of eukaryotic membranes. Dev. Cell *16*, 493–506.

Cid, V.J., Adamiková, L., Sánchez, M., Molina, M., and Nombela, C. (2001). Cell cycle control of septin ring dynamics in the budding yeast. Microbiology *147*, 1437–1450.

Cox, B.S., Tuite, M.F., and McLaughlin, C.S. (1988). The psi factor of yeast: a problem in inheritance. Yeast *4*, 159–178.

Derdowski, A., Sindi, S.S., Klaips, C.L., DiSalvo, S., and Serio, T.R. (2010). A size threshold limits prion transmission and establishes phenotypic diversity. Science *330*, 680–683.

DeWard, A.D., Eisenmann, K.M., Matheson, S.F., and Alberts, A.S. (2010). The role of formins in human disease. Biochim. Biophys. Acta *1803*, 226–233.

Dimauro, S., and Davidzon, G. (2005). Mitochondrial DNA and disease. Ann. Med. *37*, 222–232.

Dujon, B. (1981). Mitochondrial genetics and functions. In Molecular Biology of the Yeast Saccharomyces, L. Cycle, I.E.J.J. Strathern, and J. Broach, eds. (Cold Spring Harbor, NY: Cold Spring Harbor Laboratory Press), pp. 505–635.

Dujon, B., Slonimski, P.P., and Weill, L. (1974). Mitochondrial genetics IX: A model for recombination and segregation of mitochondrial genomes in saccharomyces cerevisiae. Genetics *78*, 415–437.

Erjavec, N., Larsson, L., Grantham, J., and Nyström, T. (2007). Accelerated aging and failure to segregate damaged proteins in Sir2 mutants can be suppressed by overproducing the protein aggregation-remodeling factor Hsp104p. Genes Dev. *21*, 2410–2421.

Estey, M.P., Di Ciano-Oliveira, C., Froese, C.D., Bejide, M.T., and Trimble, W.S. (2010). Distinct roles of septins in cytokinesis: SEPT9 mediates midbody abscission. J. Cell Biol. *191*, 741–749.

Ford, S.K., and Pringle, J.R. (1991). Cellular morphogenesis in the Saccharomyces cerevisiae cell cycle: localization of the CDC11 gene product and the timing of events at the budding site. Dev. Genet. *12*, 281–292.

Galiano, M.R., Jha, S., Ho, T.S., Zhang, C., Ogawa, Y., Chang, K.J., Stankewich, M.C., Mohler, P.J., and Rasband, M.N. (2012). A distal axonal cytoskeleton forms an intra-axonal boundary that controls axon initial segment assembly. Cell *149*, 1125–1139.

García-Rodríguez, L.J., Crider, D.G., Gay, A.C., Salanueva, I.J., Boldogh, I.R., and Pon, L.A. (2009). Mitochondrial inheritance is required for MEN-regulated cytokinesis in budding yeast. Curr. Biol. *19*, 1730–1735.

Greene, L.E., Park, Y.N., Masison, D.C., and Eisenberg, E. (2009). Application of GFP-labeling to study prions in yeast. Protein Pept. Lett. *16*, 635–641.

Halfmann, R., Alberti, S., Krishnan, R., Lyle, N., O'Donnell, C.W., King, O.D., Berger, B., Pappu, R.V., and Lindquist, S. (2011). Opposing effects of glutamine and asparagine govern prion formation by intrinsically disordered proteins. Mol. Cell *43*, 72–84.

Hartwell, L.H. (1971). Genetic control of the cell division cycle in yeast. IV. Genes controlling bud emergence and cytokinesis. Exp. Cell Res. *69*, 265–276.

Hermann, G.J., Thatcher, J.W., Mills, J.P., Hales, K.G., Fuller, M.T., Nunnari, J., and Shaw, J.M. (1998). Mitochondrial fusion in yeast requires the transmembrane GTPase Fzo1p. J. Cell Biol. *143*, 359–373.

Hoppins, S., Lackner, L., and Nunnari, J. (2007). The machines that divide and fuse mitochondria. Annu. Rev. Biochem. *76*, 751–780.

Hurley, J.H., and Hanson, P.I. (2010). Membrane budding and scission by the ESCRT machinery: it's all in the neck. Nat. Rev. Mol. Cell Biol. *11*, 556–566.

Ihara, M., Kinoshita, A., Yamada, S., Tanaka, H., Tanigaki, A., Kitano, A., Goto, M., Okubo, K., Nishiyama, H., Ogawa, O., et al. (2005). Cortical organization by the septin cytoskeleton is essential for structural and mechanical integrity of mammalian spermatozoa. Dev. Cell *8*, 343–352.

Jokinen, R., and Battersby, B.J. (2012). Insight into mammalian mitochondrial DNA segregation. Ann. Med. Published online July 9, 2012.

Kawai-Noma, S., Ayano, S., Pack, C.G., Kinjo, M., Yoshida, M., Yasuda, K., and Taguchi, H. (2006). Dynamics of yeast prion aggregates in single living cells. Genes Cells *11*, 1085–1096.

Kim, H.B., Haarer, B.K., and Pringle, J.R. (1991). Cellular morphogenesis in the Saccharomyces cerevisiae cell cycle: localization of the CDC3 gene product and the timing of events at the budding site. J. Cell Biol. *112*, 535–544.

Kissel, H., Georgescu, M.M., Larisch, S., Manova, K., Hunnicutt, G.R., and Steller, H. (2005). The Sept4 septin locus is required for sperm terminal differentiation in mice. Dev. Cell *8*, 353–364.

Knoblich, J.A. (2008). Mechanisms of asymmetric stem cell division. Cell *132*, 583–597.

Komarnitsky, S.I., Chiang, Y.C., Luca, F.C., Chen, J., Toyn, J.H., Winey, M., Johnston, L.H., and Denis, C.L. (1998). DBF2 protein kinase binds to and acts through the cell cycle-regulated MOB1 protein. Mol. Cell. Biol. *18*, 2100–2107.

Kucej, M., Kucejova, B., Subramanian, R., Chen, X.J., and Butow, R.A. (2008). Mitochondrial nucleoids undergo remodeling in response to metabolic cues. J. Cell Sci. *121*, 1861–1868.

Kusch, J., Meyer, A., Snyder, M.P., and Barral, Y. (2002). Microtubule capture by the cleavage apparatus is required for proper spindle positioning in yeast. Genes Dev. *16*, 1627–1639.

Lewontin, R.C. (1971). The effect of genetic linkage on the mean fitness of a population. Proc. Natl. Acad. Sci. USA *68*, 984–986.

Liebman, S.W., and Chernoff, Y.O. (2012). Prions in yeast. Genetics *191*, 1041–1072.

Lin, Y.H., Lin, Y.M., Wang, Y.Y., Yu, I.S., Lin, Y.W., Wang, Y.H., Wu, C.M., Pan, H.A., Chao, S.C., Yen, P.H., et al. (2009). The expression level of septin12 is critical for spermiogenesis. Am. J. Pathol. *174*, 1857–1868.

Lippincott, J., Shannon, K.B., Shou, W., Deshaies, R.J., and Li, R. (2001). The Tem1 small GTPase controls actomyosin and septin dynamics during cytokinesis. J. Cell Sci. *114*, 1379–1386.

Liu, J., Fairn, G.D., Ceccarelli, D.F., Sicheri, F., and Wilde, A. (2012). Cleavage furrow organization requires PIP(2)-mediated recruitment of anillin. Curr. Biol. *22*, 64–69.

Longtine, M.S., and Bi, E. (2003). Regulation of septin organization and function in yeast. Trends Cell Biol. *13*, 403–409.

Longtine, M.S., Fares, H., and Pringle, J.R. (1998). Role of the yeast Gin4p protein kinase in septin assembly and the relationship between septin assembly and septin function. J. Cell Biol. *143*, 719–736.

Lukins, H.B., Tate, J.R., Saunders, G.W., and Linnane, A.W. (1973). The biogenesis of mitochondria 26. Mitochondrial recombination: the segregation of parental and recombinant mitochondrial genotypes during vegetative division of yeast. Mol. Gen. Genet. *120*, 17–25.

Mathur, V., Seuring, C., Riek, R., Saupe, S.J., and Liebman, S.W. (2012). Localization of HET-S to the cell periphery, not to [Het-s] aggregates, is associated with [Het-s]-HET-S toxicity. Mol. Cell. Biol. *32*, 139–153.

McGlinchey, R.P., Kryndushkin, D., and Wickner, R.B. (2011). Suicidal [PSI+] is a lethal yeast prion. Proc. Natl. Acad. Sci. USA *108*, 5337–5341.

Meeusen, S., Tieu, Q., Wong, E., Weiss, E., Schieltz, D., Yates, J.R., and Nunnari, J. (1999). Mgm101p is a novel component of the mitochondrial nucleoid that binds DNA and is required for the repair of oxidatively damaged mitochondrial DNA. J. Cell Biol. *145*, 291–304.

Melloy, P., Shen, S., White, E., McIntosh, J.R., and Rose, M.D. (2007). Nuclear fusion during yeast mating occurs by a three-step pathway. J. Cell Biol. *179*, 659–670.

Merisko, E.M., Fletcher, M., and Palade, G.E. (1986). The reorganization of the Golgi complex in anoxic pancreatic acinar cells. Pancreas *1*, 95–109.

Molk, J.N., and Bloom, K. (2006). Microtubule dynamics in the budding yeast mating pathway. J. Cell Sci. *119*, 3485–3490.

Mollenhauer, H.H., and Morré, D.J. (1978). Structural compartmentation of the cytosol: zones of exclusion, zones of adhesion, cytoskeletal and intercisternal elements. Subcell. Biochem. *5*, 327–359.

Nunnari, J., Marshall, W.F., Straight, A., Murray, A., Sedat, J.W., and Walter, P. (1997). Mitochondrial transmission during mating in Saccharomyces cerevisiae is determined by mitochondrial fusion and fission and the intramitochondrial segregation of mitochondrial DNA. Mol. Biol. Cell *8*, 1233–1242.

Okamoto, K., and Shaw, J.M. (2005). Mitochondrial morphology and dynamics in yeast and multicellular eukaryotes. Annu. Rev. Genet. *39*, 503–536.

Okamoto, K., Perlman, P.S., and Butow, R.A. (1998). The sorting of mitochondrial DNA and mitochondrial proteins in zygotes: preferential transmission of mitochondrial DNA to the medial bud. J. Cell Biol. *142*, 613–623.

Paushkin, S.V., Kushnirov, V.V., Smirnov, V.N., and Ter-Avanesyan, M.D. (1996). Propagation of the yeast prion-like [psi+] determinant is mediated by oligomerization of the SUP35-encoded polypeptide chain release factor. EMBO J. *15*, 3127–3134.

Pereira, G., and Yamashita, Y.M. (2011). Fly meets yeast: checking the correct orientation of cell division. Trends Cell Biol. *21*, 526–533.

Pruyne, D., Gao, L., Bi, E., and Bretscher, A. (2004). Stable and dynamic axes of polarity use distinct formin isoforms in budding yeast. Mol. Biol. Cell *15*, 4971–4989.

Rando, T.A. (2006). Stem cells, ageing and the quest for immortality. Nature *441*, 1080–1086.

Rujano, M.A., Bosveld, F., Salomons, F.A., Dijk, F., van Waarde, M.A., van der Want, J.J., de Vos, R.A., Brunt, E.R., Sibon, O.C., and Kampinga, H.H. (2006). Polarised asymmetric inheritance of accumulated protein damage in higher eukaryotes. PLoS Biol. *4*, e417.

Satpute-Krishnan, P., and Serio, T.R. (2005). Prion protein remodelling confers an immediate phenotypic switch. Nature *437*, 262–265.

Saupe, S.J. (2011). The [Het-s] prion of Podospora anserina and its role in heterokaryon incompatibility. Semin. Cell Dev. Biol. *22*, 460–468.

Seiser, R.M., Sundberg, A.E., Wollam, B.J., Zobel-Thropp, P., Baldwin, K., Spector, M.D., and Lycan, D.E. (2006). Ltv1 is required for efficient nuclear export of the ribosomal small subunit in Saccharomyces cerevisiae. Genetics *174*, 679–691.

Serio, T.R., and Lindquist, S.L. (1999). [PSI+]: an epigenetic modulator of translation termination efficiency. Annu. Rev. Cell Dev. Biol. *15*, 661–703.

Seshan, A., and Amon, A. (2004). Linked for life: temporal and spatial coordination of late mitotic events. Curr. Opin. Cell Biol. *16*, 41–48.

Shcheprova, Z., Baldi, S., Frei, S.B., Gonnet, G., and Barral, Y. (2008). A mechanism for asymmetric segregation of age during yeast budding. Nature *454*, 728–734.

Slaughter, B.D., Das, A., Schwartz, J.W., Rubinstein, B., and Li, R. (2009). Dual modes of cdc42 recycling fine-tune polarized morphogenesis. Dev. Cell *17*, 823–835.

Song, A.H., Wang, D., Chen, G., Li, Y., Luo, J., Duan, S., and Poo, M.M. (2009). A selective filter for cytoplasmic transport at the axon initial segment. Cell *136*, 1148–1160.

Spiliotis, E.T., and Gladfelter, A.S. (2012). Spatial guidance of cell asymmetry: septin GTPases show the way. Traffic *13*, 195–203.

Spokoini, R., Moldavski, O., Nahmias, Y., England, J.L., Schuldiner, M., and Kaganovich, D. (2012). Confinement to organelle-associated inclusion structures mediates asymmetric inheritance of aggregated protein in budding yeast. Cell Rep. *2*, 738–747.

Steigemann, P., Wurzenberger, C., Schmitz, M.H., Held, M., Guizetti, J., Maar, S., and Gerlich, D.W. (2009). Aurora B-mediated abscission checkpoint protects against tetraploidization. Cell *136*, 473–484.

Stein, M., Wandinger-Ness, A., and Roitbak, T. (2002). Altered trafficking and epithelial cell polarity in disease. Trends Cell Biol. *12*, 374–381.

Strausberg, R.L., and Perlman, P.S. (1978). The effect of zygotic bud position on the transmission of mitochondrial genes in Saccharomyces cerevisiae. Mol. Gen. Genet. *163*, 131–144.

Tartakoff, A.M., and Jaiswal, P. (2009). Nuclear fusion and genome encounter during yeast zygote formation. Mol. Biol. Cell *20*, 2932–2942.

Thomas, D.Y., and Wilkie, D. (1968). Recombination of mitochondrial drug-resistance factors in Saccharomyces cerevisiae. Biochem. Biophys. Res. Commun. *30*, 368–372.

Togneri, J., Cheng, Y.S., Munson, M., Hughson, F.M., and Carr, C.M. (2006). Specific SNARE complex binding mode of the Sec1/Munc-18 protein, Sec1p. Proc. Natl. Acad. Sci. USA *103*, 17730–17735.

Tyedmers, J., Treusch, S., Dong, J., McCaffery, J.M., Bevis, B., and Lindquist, S. (2010). Prion induction involves an ancient system for the sequestration of aggregated proteins and heritable changes in prion fragmentation. Proc. Natl. Acad. Sci. USA *107*, 8633–8638.

Uptain, S.M., Sawicki, G.J., Caughey, B., and Lindquist, S. (2001). Strains of [PSI(+)] are distinguished by their efficiencies of prion-mediated conformational conversion. EMBO J. *20*, 6236–6245.

Vishveshwara, N., Bradley, M.E., and Liebman, S.W. (2009). Sequestration of essential proteins causes prion associated toxicity in yeast. Mol. Microbiol. *73*, 1101–1114.

Weisman, L.S. (2006). Organelles on the move: insights from yeast vacuole inheritance. Nat. Rev. Mol. Cell Biol. *7*, 243–252.

Wickner, R.B., Edskes, H.K., Shewmaker, F., and Nakayashiki, T. (2007). Prions of fungi: inherited structures and biological roles. Nat. Rev. Microbiol. *5*, 611–618.

Wickner, R.B., Shewmaker, F., Edskes, H., Kryndushkin, D., Nemecek, J., McGlinchey, R., Bateman, D., and Winchester, C.L. (2010). Prion amyloid structure explains templating: how proteins can be genes. FEMS Yeast Res. *10*, 980–991.

Wolosewick, J.J., and Porter, K.R. (1979). Microtrabecular lattice of the cytoplasmic ground substance. Artifact or reality. J. Cell Biol. *82*, 114–139.

Yang, H.C., and Pon, L.A. (2002). Actin cable dynamics in budding yeast. Proc. Natl. Acad. Sci. USA *99*, 751–756.